

oil-induced spectral shift of each resonant peak of the LPG. The error bar is smaller than the size of the data point.

Secondly, we mechanically scratched the surface of the fibre and investigated the spectral change of the LPG. As mentioned earlier, coupling to a cladding mode is possible only when the cladding can support the mode; hence, the loss peaks of an LPG are expected to be removed by the scratching. The fibre embedding the LPG was glued onto a slide glass using a Norland UV curable adhesive, and the top surface was rubbed with #800 sandpaper. As expected, each peak loss of the LPG was reduced following the scratching, but no appreciable change in the first peak was observed. The spectra of the LPG before scratching (curve (i)) and after scratching (curve (ii)), are shown in Fig. 3.

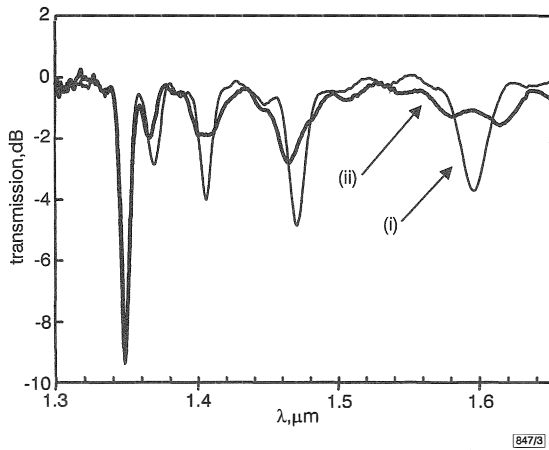


Fig. 3 Transmission spectra of LPG measured before and after mechanical scratching

(i) before scratching
(ii) after scratching

The fibre embedding the LPG was glued on a slide glass and the top surface was rubbed with sandpaper

Results and discussion: The LPG written in a DSC type DSF had a strong peak in the short wavelength region of the transmission spectrum, and this peak was not sensitive to the cladding-surrounding interface. From the second peak, as usual, the coupling intensity increased as the mode order increased, and their peak wavelengths and peak depths were changed when the grating was immersed in index matching oil or when the grating surface was scratched. Therefore, it is considered that the strong first peak might result from coupling to an internal cladding mode, weakly guided by the inner cladding layer of the DSC type fibre, or that the inner cladding layer strongly modifies the field profile of the first cladding mode. The rather flat spectral loss in the long wavelength region of curve (ii) of Fig. 1 is thought to result from the coupling to a continuum radiation mode [1]. In scratching the LPG, we scratched only the top surface of the cladding for the sake of experimental simplicity. The other azimuthal part of the cladding was interfaced with the adhesive used to fix the fibre onto a slide glass. Owing to the thickness and flexibility of the adhesive, part of the spectral degradation of curve (ii) of Fig. 3 might have resulted from bending of the fibre, which was unintentionally induced during rubbing.

This LPG without cladding-surrounding interface has applications in telecommunications devices. Because a fibre without a coating layer is mechanically weak and easily contaminated, re-coating the fibre after making a fibre grating is generally required. In this case, the LPG device using the first peak of the LPG written in a DSC type fibre has an advantage over the conventional LPG device, which uses a high order mode and is sensitive to the cladding-surrounding interface.

Conclusions: We presented the resonance peak of an LPG without, or with less, sensitivity to the interface between the cladding and its surrounding media. The first peak of the LPG written in a DSC type DSF was not sensitive to index matching oil applied on the cladding surface but also to scratching on the cladding surface. The strong first resonant peak of the LPG can be utilised in making devices for telecommunications systems which require less sensitivity to the fibre surroundings, such as re-coating or contamination on the cladding surface.

Acknowledgment: The authors are grateful to T. Erdogan of the University of Rochester for useful discussions.

© IEE 1998

Electronics Letters Online No: 19980788

6 April 1998

B.H. Lee and J. Nishii (Osaka National Research Institute, AIST, 1-8-31 Midorigaoka, Ikeda, Osaka 563-8577, Japan)

References

- 1 ERDOGAN, T.: 'Fiber grating spectra', *J. Lightwave Technol.*, 1997, **LT-15**, (8), pp. 1277-1294
- 2 PATRICK, H.J., KERSEY, A.D., BUCHOLTZ, F., EWING, K.J., JUDKINS, J.B., and VENSGARKAR, A.M.: 'Chemical sensor based on long-period fiber grating response to index of refraction'. Proc. of Conf. on Lasers and Electro-Optics, 1997, pp. 420-421
- 3 LEE, B.H., LIU, Y., LEE, S.B., CHOI, S.S., and JANG, J.N.: 'Displacements of the resonant peaks of a long-period fiber grating induced by a change of ambient refractive index', *Opt. Lett.*, 1997, **22**, (23), pp. 1769-1771
- 4 KUWAKI, N., OHASHI, M., TANAKA, C., UESUGI, N., SEIKAI, S., and NEGISHI, Y.: 'Characteristics of dispersion-shifted dual shape core singlemode fibers', *J. Lightwave Technol.*, 1987, **LT-5**, (6), pp. 792-797

Experimental evaluation of broadband isotropic electric field sensor using three Mach-Zehnder interferometers

K. Tajima, R. Kobayashi and N. Kuwabara

A new isotropic electric field sensor integrating three Mach-Zehnder interferometers into one small case has been developed. The three small printed dipole antennas are mutually orthogonal. Experimental measurements showed high sensitivity, wide frequency range and an ideal directional pattern.

Introduction: Some kinds of electric field sensors using optical modulators (an optical E-field sensor) have been developed recently in order to evaluate field strength or distribution in electromagnetic compatibility (EMC) measurements [1-3]. However, an isotropic sensor is needed because polarisations of electromagnetic waves are not always uniform in real environments, such as electrostatic discharge and the near field around a cellular telephone.

This Letter presents the measured characteristics of a new compact isotropic electric field (E-field) sensor using optical modulators. The directional pattern of this sensor is isotropic because it has three printed dipole antennas in a mutually orthogonal configuration. The frequency bandwidth is very broad, DC to 10GHz and the maximum sensitivity is 87dB ($\mu\text{V}/\text{m}$) (= 22mV/m). Moreover, the resolution for measuring electric field strength is very high because the sensor element is very small, only 8mm long.

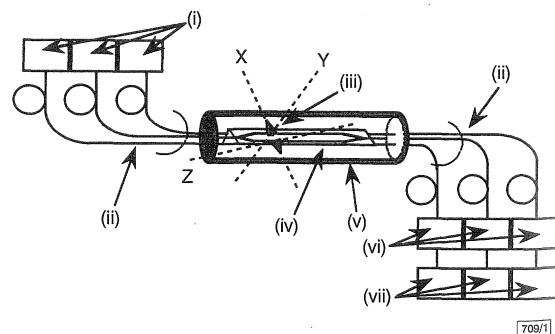


Fig. 1 Structure of isotropic optical E-field sensor

- (i) LD-pumped YAG laser
- (ii) polarisation maintaining fibre: 30 m
- (iii) sensor element
- (iv) teflon case
- (v) optical modulator (Mach-Zehnder interferometer)
- (vi) photodetectors
- (vii) spectrum analysers

Structure of sensor: The structure of the isotropic optical E-field sensor is shown in Fig. 1. The sensing part consists of three Mach-Zehnder interferometers mounted on each surface of a triangular pole and the outside case, which is 150mm long and 50mm in diameter, is made of teflon. Each of the sensor elements is an 8mm long dipole antenna, consisting of two pieces of 0.5mm thick glass plate with a 150Å thick tapered (0.5mm at the base, 4mm high) nichrome film is attached to its optical modulator at an angle of 54.7° with respect to the optical waveguide [4]. In this structure, the elements are set to be mutually orthogonal along the x , y and z axes. The Mach-Zehnder interferometer was formed by Ti diffusion on a Z-cut LiNbO₃ substrate 55mm long, 1mm wide, and 0.5mm thick. The light source was a 1.3µm LD pumped YAG laser (25mW) and the photodetector was a *pin* photodiode (HP1198: DC-15GHZ). The connections between the light source and the E-field sensor, and between the E-field sensor and the photodetector, were made with a 30m long polarisation-maintaining fibre. The optical signal modulated by an external electric field in the modulator was changed to an electrical signal in the photodetector, and the signal was measured with a spectrum analyser.

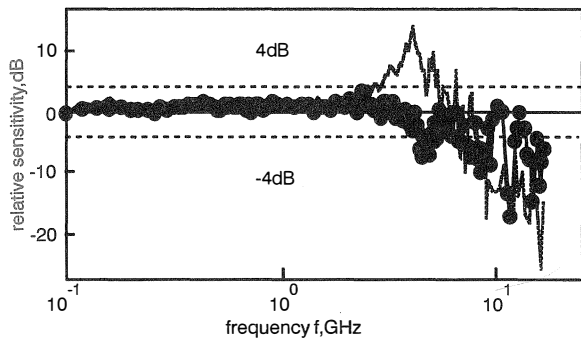


Fig. 2 Frequency response

Element length: 8mm
 ● measured (new)
 --- measured (conventional)

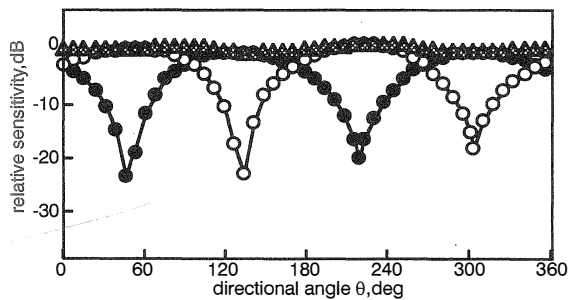


Fig. 3 Directional pattern of isotropic optical E-field sensor in plane including element

$f = 1.9\text{GHz}$
 ● y -axis
 ○ z -axis
 ▲ total

Experimental results: The measured frequency characteristics are shown in Fig. 2. In this Figure, the horizontal axis shows frequency, 100MHz to 15GHz, and the vertical axis shows the relative output voltage under 10V/m, normalised by the values at 100MHz. The measurement was carried out using a GTEM cell, with electric field strength calibrated using an electric field probe (EMCO Model 7121). Fig. 2 shows that the sensitivity of the sensor was constant within $\pm 4\text{dB}$ at frequencies up to 6GHz. Although its sensitivity decreased by 10dB at 10GHz, this sensor can be used at frequencies up to 10GHz. The thin solid line is the response of the conventional sensor [5], which exhibits resonance at 4.5GHz and has a gain of more than 10dB. In this new sensor, the frequency characteristics were improved by optimising resistive elements using the method of moments [6].

The output voltages of the optical detector were measured at 1.5, 1.9, and 2.5GHz under various applied electric field strengths in the GTEM cell, where the electric field strength was varied

from 84 to 158dB ($\mu\text{V/m}$) (measurement limit). The results at the three frequencies were close to each other. The dynamic range was $> 70\text{dB}$, the antenna factor was 87dB, and the minimum detectable electric field strength was 87dB ($\mu\text{V/m}$) ($= 22\text{mV/m}$). The sensitivity obtained by a commercial E-field sensor, with an element of almost the same size, was 2V/m, indicating that our sensor is 100 times more sensitive.

The directional characteristics were measured in a semi-anechoic chamber with 30cm thick RF absorbers on its conductive ground plane. A horizontally-polarised wave was applied from a horn antenna 3m away from the sensor, with its x -axis element placed vertically and the turn-table was rotated every 15° (total rotation of 360°). Fig. 3 shows the directional pattern of the sensor. The output voltages of only the y -axis (●) and z -axis (○) were measured, because that of the x -axis was nearly the noise floor level. In this Figure, the vertical axis is the relative output voltage, and the maximum value of the y -axis was used for reference (0dB). The total electric field strength of the three directions is given by

$$E_{total} = \sqrt{E_x^2 + E_y^2 + E_z^2} \quad (1)$$

where E_x , E_y , and E_z are the components of the electric field strength along the x , y and z -axes, respectively. The measured results show that the directional characteristics of the total electric field were almost isotropic and the sensitivity deviations were within $\pm 1\text{dB}$ for any direction. The pattern of each element was similar to that of a tuned dipole antenna.

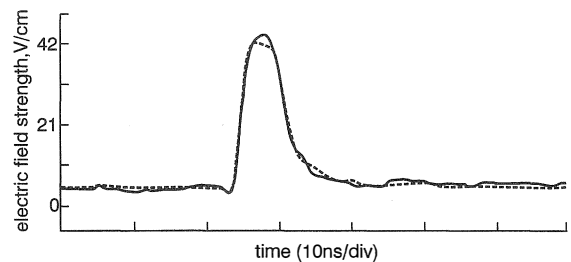


Fig. 4 Response for nanosecond impulse

--- applied electric field
 — response

This sensor is useful for measuring electromagnetic pulses generated by electrostatic discharge. An example is shown in Fig. 4. A 10ns wide impulse was measured by this new sensor in a TEM cell whose bandwidth was 1GHz. The waveform measured by the sensor was almost the same as the applied waveform.

Conclusion: Some characteristics of a new isotropic optical E-field sensor were presented. This new sensor has a broad bandwidth which is more than twice that of the conventional optical E-field sensor, as a result of optimising the sensor element. It also has good sensitivity, ~ 100 times that of a commercial E-field sensor, ideal directional characteristics as an isotropic antenna, and fast response to a 10ns impulse.

Acknowledgments: The authors would like to thank all the EMC group members for their helpful discussion. We would also like to thank H. Yamamoto for his encouragement.

© IEE 1998

15 April 1998

Electronics Letters Online No: 19980760

K. Tajima, R. Kobayashi and N. Kuwabara (EMC Research Group, Network Integrity Laboratory, NTT Multimedia Networks Laboratories, 3-9-11 Midori-cho Musashino-shi, Tokyo 180-8585, Japan)

References

- 1 KUWABARA, N., and KOBAYASHI, R.: 'Development of electric field sensor using Mach-Zehnder interferometer'. Proc. 11th International Zurich Symp. on EMC, 1995, Switzerland, pp. 489-494

- 2 GASSMANN, F., and MAILAND, M.: 'A 9 channel photonic isotropic electric and magnetic field sensor with subnanosecond rise time'. Proc. 12th International Zurich Symp. on EMC, 1997, Switzerland, pp. 217-221
- 3 SCHWERDT, M., BERGER, J., and PETERMANN, K.: 'An integrated optical E-field sensor using a reflection scheme'. Proc. 12th International Zurich Symp. on EMC, 1997, Switzerland, pp. 597-602
- 4 KANDA, M., and DRIVER, L.D.: 'An isotropic electric-field probe with tapered resistive dipoles for broadband use, 100kHz to 18GHz'. *IEEE Trans. Microw. Theory Tech.*, 1987, **MTT-35**, (2), pp. 124-130
- 5 TAJIMA, K., KUWABARA, N., KOBAYASHI, R., and TOKUDA, M.: 'Evaluation of electric field sensor with very small element using Mach-Zehnder interferometer'. *Trans. IEICE*, 1996, **79-B-II**, (11), pp. 744-753 (in Japanese)
- 6 TAJIMA, K., KOBAYASHI, R., KUWABARA, N., and TOKUDA, M.: 'Frequency bandwidth improvement of electric field sensor using optical modulator by resistively loaded element'. *Trans. Inst. Electr. Eng. Jpn.*, 1997, **117-A**, (5), pp. 515-522 (in Japanese)

Theory: A grating period is composed of an unperturbed region and a perturbed region. The transfer matrix of the unperturbed region is simply

$$T_u = \begin{bmatrix} e^{-j\beta_1 L_1} & 0 \\ 0 & e^{-j\beta_2 L_1} \end{bmatrix}$$

where L_1 is the length of the unperturbed region. In the perturbed region, the guided fundamental mode couples with the forward propagating cladding mode according to the phase matching condition $\Lambda = 2\pi/(\beta_1 - \beta_2)$, where Λ is the grating period and β_1 , and β_2 are the propagating constants which can be obtained by numerically solving the dispersion equation of a doubly-clad fibre [9]. The coupled-mode equations in the perturbed region are as follows [10]:

$$\begin{aligned} dA_1/dz &= -j\beta_1 A_1 + jC A_2 \\ dA_2/dz &= jC A_1 - j\beta_2 A_2 \end{aligned}$$

where A_1 and A_2 are the amplitudes of the two coupling modes. C is the coupling coefficient. By solving the equation, we obtain the transfer matrix of the perturbed region:

$$T_p = \begin{bmatrix} f_{11} & f_{12} \\ f_{21} & f_{22} \end{bmatrix}$$

where

$$\begin{aligned} f_{11} &= \frac{1}{2} \left[1 - (1+Q^2)^{-\frac{1}{2}} \right] e^{-jh_1 L_2} + \frac{1}{2} \left[1 + (1+Q^2)^{-\frac{1}{2}} \right] e^{-jh_2 L_2} \\ f_{21} &= \frac{1}{2} \left[1 + Q^{-2} \right]^{-\frac{1}{2}} (e^{-jh_1 L_2} - e^{-jh_2 L_2}) \\ f_{12} &= \frac{1}{2} \left[1 + Q^{-2} \right]^{-\frac{1}{2}} (e^{-jh_1 L_2} - e^{-jh_2 L_2}) \\ f_{22} &= \frac{1}{2} \left[1 + (1+Q^2)^{-\frac{1}{2}} \right] e^{-jh_1 L_2} + \frac{1}{2} \left[1 - (1+Q^2)^{-\frac{1}{2}} \right] e^{-jh_2 L_2} \end{aligned}$$

Here, $Q = 2C/(\beta_1 - \beta_2)$, $h_1 = (\beta_1 + \beta_2)/2 + C\sqrt{1+(1/Q^2)}$, and L_2 is the length of the perturbed region. The transfer matrix of one grating period is $T_n = T_p \times T_u$ while the transfer matrix of the whole grating is simply the cascade of the transfer matrices of all the grating periods:

$$T = \begin{bmatrix} t_{11} & t_{12} \\ t_{21} & t_{22} \end{bmatrix} = T_n \times T_{n-1} \times \dots \times T_1$$

and the power transmission of the fundamental mode is $|t_{11}|^2$.

In this Letter, we introduce a phase shift into the grating by adding length of unperturbed region into the middle of the grating. From the phase matching condition we can see that by adding a length Λ we get a phase shift of 2π , by adding a length of $\Lambda/2$, we get a phase shift of π , and so on. To obtain the transfer matrix of this phase shifted grating, we only need to add a matrix

$$T_s = \begin{bmatrix} e^{-j\beta_1 L} & 0 \\ 0 & e^{-j\beta_2 L} \end{bmatrix}$$

into the middle of the above cascade of transfer matrices. Here, L is the length of the region added into the grating. The result is $T = T_n \dots T_{n/2} \cdot T_s \cdot T_{n/2-1} \dots T_1$.

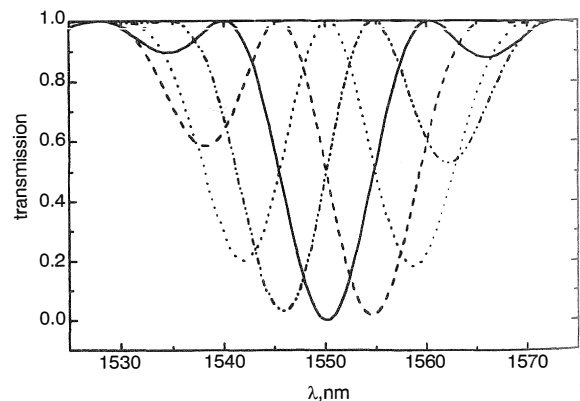


Fig. 1 Transmission spectra of phase-shifted LPG

- B
- - - C
- D
- · - · E

Gain flattening fibre filters using phase-shifted long period fibre gratings

J.R. Qian and H.F. Chen

The transmission characteristics of phase-shifted long period gratings (LPGs) are examined theoretically by a combination of coupled-mode theory and transfer matrix formulation. It is shown that the transmission spectrum of such a grating can be significantly controlled by the phase shift which allows the shape of the spectrum to be tailored to meet the requirements of many kinds of gain flattening. By choosing the phase shift and the index change appropriately, a phase-shifted LPG is designed to flatten the spectrum of an Er:silica superfluorescent fibre source.

Introduction: The gain flattening filter has aroused great interest recently, mainly because of the unprecedented increase in the demand for transmission capacity. The usable bandwidth of the signal spectrum can be significantly increased by using amplifiers with a flattened gain spectrum [1]. There are two basic ways to flatten the gain spectrum: one is to tailor the material properties of the erbium-doped fibre, and the other is to use filters designed to approximate the inverse characteristics of the gain spectrum [2]. Since this kind of filter requires transmission characteristics of very low back reflection and wide bandwidth, long period grating (LPG) devices which operate in the transmission mode have found a role in these applications because of their good performance [3]. The LPG is a type of transmission grating based on the principle of coupling the guided fundamental mode to the forward propagating lossy cladding modes. Unlike their Bragg counterparts, the refractive index perturbations of LPGs have a much greater periodicity than the wavelength of the light, which allows this kind of grating to be easily manufactured [4]. In recent years, LPGs have found numerous applications in mode convertors [5], fibre sensors [6], gain flattening filters [7] and band rejection filters [8]. Normally, the spectrum of an LPG has only one dip, and although changing the parameters of the grating can tailor the shape of this dip, it can only flatten one of the peaks in the gain spectrum at a time. To flatten all the peaks in the spectrum, a series of LPGs have to be chained together. We note that, by introducing a phase shift in the middle of an LPG, the transmission spectrum changes from one dip to two dips and the shape of these two dips can be well controlled by changing the phase shift. Hence, by choosing a different phase shift, different shapes of LPGs spectrum may be obtained to almost fully flatten the gain spectrum with only one grating.

In this Letter, we use a combination of coupled-mode theory and the transfer matrix method to obtain the transmission spectrum of a phase-shifted LPG. This method is also capable of analysing almost any kind of nonuniform grating. After examining the way the transmission spectrum changes with different phase shifts, we design a phase-shifted LPG to flatten a practical gain spectrum which has two peaks.